

Experimental observation of few-layers MoS₂ semiconductor-to-metal transition under tensile strain

Igor Neri and Miquel López-Suárez

*NiPS Laboratory, Dipartimento di Fisica e Geologia,
Università degli Studi di Perugia, 06123 Perugia, Italy**

(Dated: October 3, 2016)

Abstract

The engineering through strain of material properties is very interesting for a wide list of applications, specially for atomically thin membranes made of MoS₂ because of its high Young modulus and fracture strength. The modification of the electronic structure and electronic transport under tensile and compressive strain of MoS₂ and other transition metal dichalcogenides has been predicted by *ab initio* calculations in several works. A transition from semiconductor to metallic transport has been predicted for single and few layer MoS₂. In this article we present the observation of this effect on a few layer MoS₂ ribbon under a maximum uniaxial tensile strain of 0.14. Experimental data are accompanied with *ab initio* calculations showing that uniaxial strain on few layer MoS₂ provokes the closing of the energy band-gap.

Molybdenum disulphide, MoS_2 , is a layered crystalline solid with an hexagonal structure similar to graphene. Single layer MoS_2 is formed by a plane of Mo atoms sandwiched and covalently bonded to two planes of S atoms. Few layer and bulk MoS_2 is formed by successive stacking of this hexagonal structure through vdW forces. In a bulk form, MoS_2 is an indirect semiconductor with energy gap $E_g=1\text{ eV}$ while its single layer counterpart shows a direct transition at the K point with $E_g=1.9\text{ eV}$. This material among other transition metal dichalcogenides (TMDs) has been widely studied in the last years because of their outstanding optical, mechanical and electrical properties along very strong electro-mechanical and opto-mechanical coupling[1–3]. In particular, MoS_2 has been suggested to show a transition from semiconductor to metal under mechanical strain[4–7] and not only for monolayer MoS_2 but also for few-layer MoS_2 and even bulk[8, 9]. Although several studies based on *ab initio* calculations have predicted this particular effect no experimental validation has been published until now.

In this letter we report the evidence of the semiconductor-metal transition of MoS_2 under tensile strain. In particular, changes in the direct-current electronic transport properties of MoS_2 are characterized for a $10\text{ }\mu\text{m}$ length MoS_2 suspended ribbon under uniaxial tensile strain up to $\varepsilon=0.14$. The transition, that occurs at $\varepsilon \approx 0.12$, is seen as a drastic increment in the current flowing through the device which is related to the closure of the gap that, typically, semiconductors show in their two terminal I-V curve. First principles band structure calculations of the material are then performed to corroborate the experimental data. The results shown in this letter paves the way for the development of new micro and nanodevices exploiting the strong electro-mechanical coupling of MoS_2 such as strain sensors, straintronic devices, among others.

MoS_2 flakes are obtained by mechanical exfoliation from a single crystal [10, 11] with the “scotch tape method” and then transferred to a polydimethylsiloxane (PDMS) holder as in Ref. [12]. An optical microscope is used to locate few layer MoS_2 candidates for the analysis. In particular we focused our attention on the flake reported in Fig. 1(a). To determine the number of layers composing the structure we have performed an optical analysis considering the light transmittance of single-layer MoS_2 to be 94.5% [13]. Increasing the number of layer the transmittance decrease linearly proportional to the number of layers, n [13]. The analysis for the selected flake is reported in Fig. 1(b), where the transmittance profile is relative to the section highlighted in Fig. 1(a). Each horizontal gray line is relative to the expected

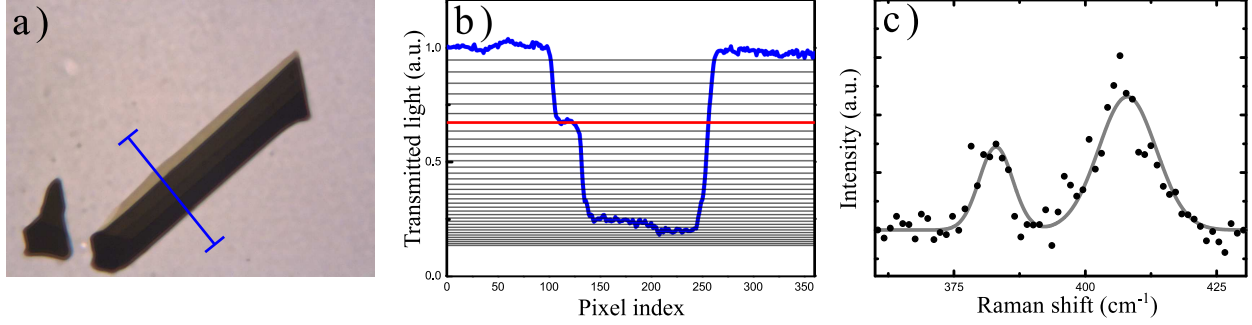


FIG. 1. Selected MoS₂ flake and results of relative optical and micro Raman analysis. a) Optical image of the selected flake: the darker portion is relative to bulk material while the lighter is for few layers MoS₂. b) Optical analysis of the highlighted section of the flake based on the light transmittance of single layer MoS₂ to estimate the number of layers. c) Micro Raman spectrum of the lighter part of the flake showing the E_{2g}^1 and A_{1g} peaks. From the relative intensity and distance between them we have estimated the number of layers of the flake to be $n=7$.

transmitted light for a specific number of layers starting from the top line corresponding to single layer, $n=1$. The red curve corresponds to the transmitted light of a 7-layers MoS₂, matching the data obtained for the lighter part of the flake reported in Fig. 1(a). We also performed Raman analysis to further characterize the sample. MoS₂ shows two peaks in the Raman spectrum, E_{2g}^1 and A_{1g} , the position and intensity of which have been demonstrated to be indicators of the number of layers [14, 15]. Fig. 1(c) shows the measured spectrum for the present device (points) excited by 532 nm line and a double Gaussian fitted curve (line) centered at 383 cm^{-1} and 407 cm^{-1} which is in good agreement with Ref. 14 for $n=7$. The relative intensity is $I_{E_{2g}^1}/I_{A_{1g}} = 0.6$, also supporting $n=7$.

In order to characterize the semiconductor-to-metal transition of a seven layer MoS₂ ribbon, we have carried out first principles calculations within Density Functional Theory (DFT) to investigate the electronic band structure of the material. We used the Siesta package [16], norm-conserving pseudopotentials and the Perdew-Burke-Eznerhof parameterization (PBE) of the Generalized Gradient Approximation (GGA) [17] to obtain the electronic structure of infinite seven layer MoS₂. An optimized double- ζ polarized basis set to expand the one-electron wave-function is considered. A $15 \times 15 \times 10$ grid of k-points to sample the Brillouin zone is used and the structure is relaxed until all forces are lower than 0.03 eV \AA^{-1} . The unit-cell of stacked MoS₂ is shown in Fig. 2(a). The values for the energy

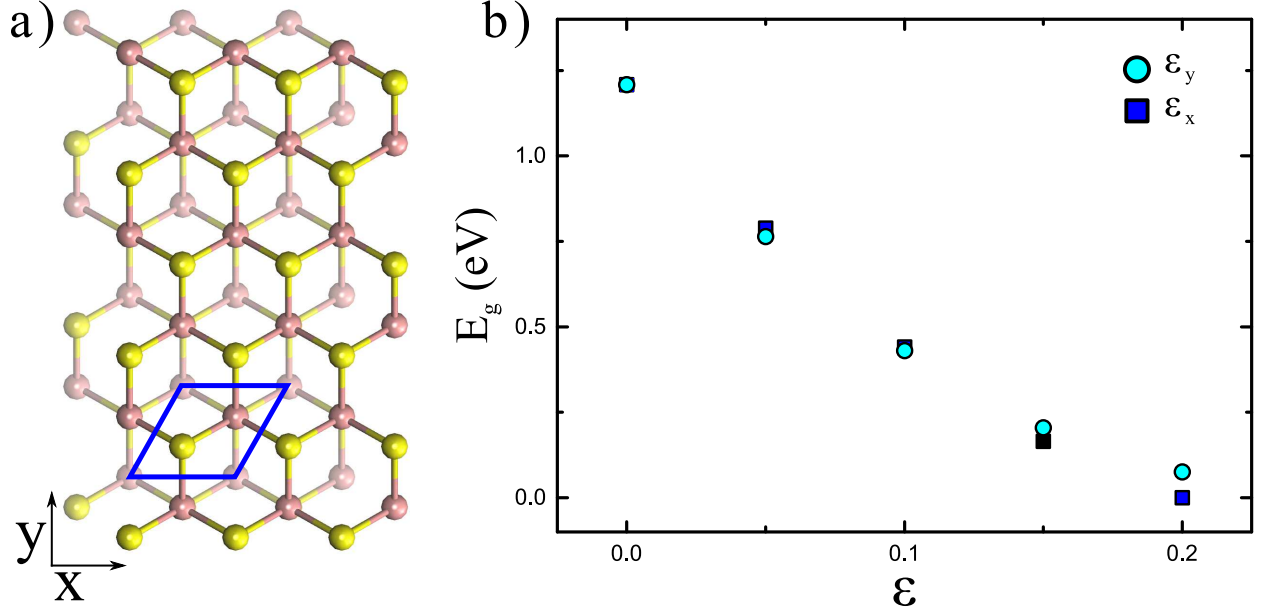


FIG. 2. Atomic structure and band-gap of multi-layer MoS₂. a) Atomic structure of stacked MoS₂ in the x-y plane, showing bonding between Mo and S atoms. b) Energy gap of seven layer MoS₂ as function of applied uniaxial strain along x and y directions.

gap ($E_g=1.06$ eV) and the lattice constant ($a=3.18$ Å) are in good agreement with those in the literature[9, 18, 19]. Strain is introduced to the system by deforming the unit cell along the zig-zag (x-axis) and arm-chair (y-axis) direction, so $\epsilon_{\{x,y\}} = \frac{\delta_{\{x,y\}}}{L_{\{x,y\}}}$. The evolution of the energy band-gap under tensile strain is shown in Fig. 2(c) decreases as the strain increases. However, one should note that, while predictions of the pressure coefficients based on DFT calculations are very reliable, the band-gaps are notoriously underestimated. Therefore, data shown in Fig. 2 (b) represent just a trend of E_g .

To test the semiconductor to metal transition in our experiment the selected flake has been transferred over a Au/Cr coated (55 nm) 500 μm SiO₂ substrate. The hospital substrate has been mounted on a high precision nanopositioning stage clamping one end of the substrate to the reference frame and the other to the movable part. The positioning system is capable of a maximum extension of 35 μm with a pull force of 10 N. Thanks to a incision made on the bottom of the substrate the force applied by the stage during elongation is capable of producing a clean crack and split it into two movable parts separated by a gap g . Once the substrate is split in two parts the flake is transferred over the trench. The initial gap was set to $g_0 \approx 10$ μm determining the length of the metal-semiconductor-metal (MSM) device

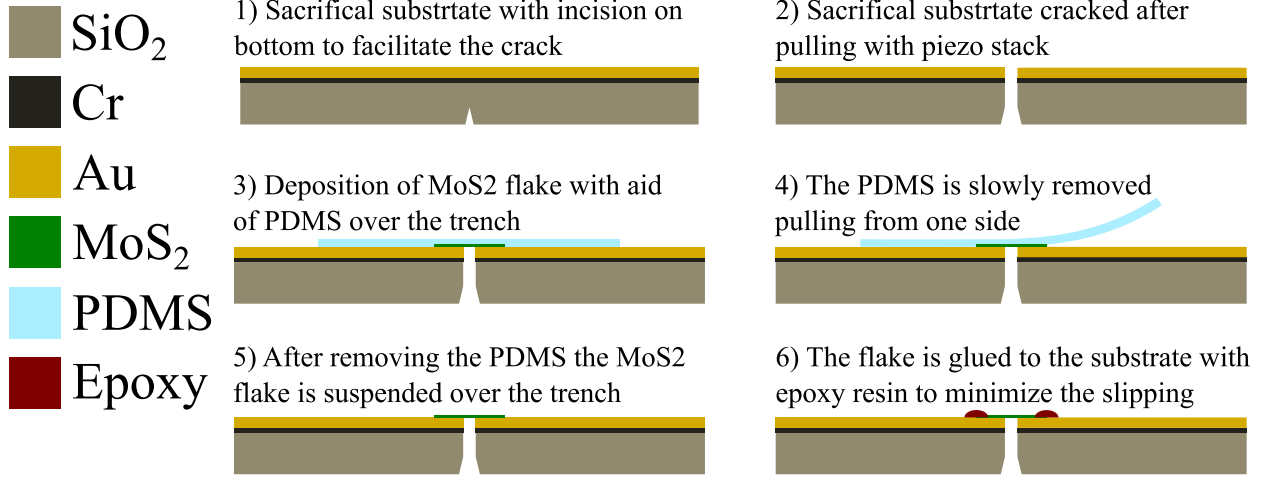


FIG. 3. Schematic representing the preparation of the hospital substrate and deposition of the MoS_2 flake.

to $l = 10 \mu\text{m}$. After the MoS_2 ribbon is transferred, two blobs of epoxy resin mechanically fix both clamps of the ribbon preventing slipping during strain application. The complete procedure of substrate preparation and transfer of the flake is depicted in detail in Fig. 3.

Strain is applied to the MSM device by increasing the gap, g , being $\varepsilon = \frac{g}{g_0} - 1$. The effective value of the gap is directly measured through the integrated positioning sensor of the linear actuator.

A possible way to directly observe semiconductor to metal transition under tensile strain is monitoring the current flowing through the material varying the polarization V_p in a two terminal configuration, *i.e.*, the I-V curve. The typical semiconductor behavior is observed in the suspended unstrained ($\varepsilon = 0.00$) MoS_2 flake, the I-V curve in this condition is represented by the green curve in Fig. 4(a). In this scenario the current remains low for $V_p < 0.2 \text{ V}$. Under tensile strain, the current flowing through the flake increases even for $|V_p| < V_{th}$, increasing substantially the slope of the curve from $0.07 \mu\text{A V}^{-1}$ to $1.1 \mu\text{A V}^{-1}$ and reaching a linear relation, which corresponds to a metallic behavior (Red curve of Fig. 4(a)). The lighter curves presented in Fig. 4(a) are relative to intermediate strains between those relative to green and red curves. After increasing the strain beyond $\varepsilon = 0.014$ the 7 layer ribbon broke and only the bulk part remained. The contribution from the bulk MoS_2 part of the flake has been then measured and is represented by the dashed line in Fig. 4(a). In this case no change on the I-V curve was measured as g increased. The I-V curves for

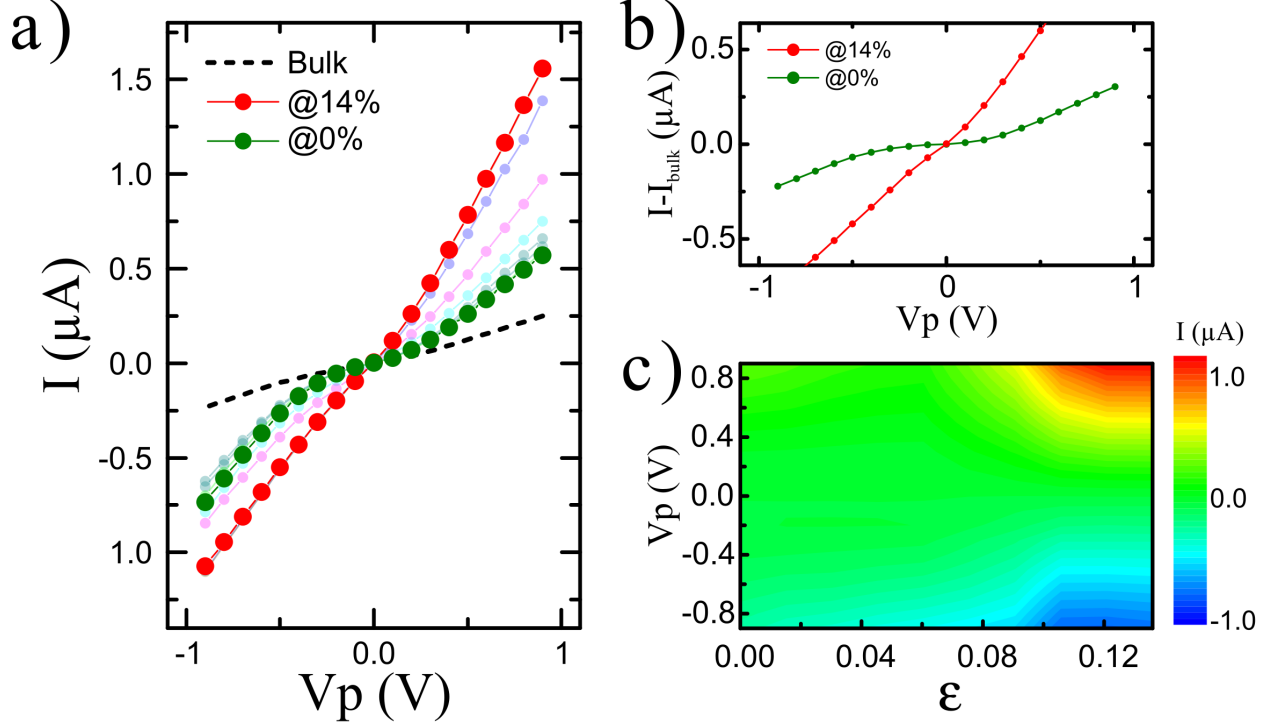


FIG. 4. Current voltage relation as function of applied tensile strain. a) I-V characteristic curve of the measured device for different applied tensile strains. b) I-V characteristic curve of the unstrained and strained device removing the static contribution of the bulk material. c) Color map of the current flowing through the device as function of polarization voltage and applied strain.

unstrained and strained device subtracting the static contribution of the bulk part of the ribbon are presented in Fig. 4(b). Fig. 4(c) show a color map of the current flowing through the device as function of applied strain and polarization voltage, showing an increase in current as function of the voltage for higher applied tensile strains.

In Fig. 5(a) the equivalent circuit of the measured device is presented. R_C represents the contact resistance, Z_b the background impedance that accounts for the bulk MoS_2 and parasitic currents. Finally, $Z_{\text{MoS}_2}(\epsilon)$ is the strain dependent impedance of the seven layer MoS_2 . According to this model the total conductance of the device can be expressed as:

$$G(\epsilon) = \frac{G_R (G_{\text{MoS}_2}(\epsilon) + G_b)}{G_R + G_{\text{MoS}_2}(\epsilon) + G_b} \quad (1)$$

where the conductance G_x is the inverse of the impedance Z_x . We now focus on the conductance of the seven layer MoS_2 . According to Ref. [20] the conductance of a semiconductor

TABLE I. Fitted parameters from the conductance model.

Parameter	Value
R_C	2.2 M Ω
Z_b	42.9 M Ω
G_0	5.54×10^{-10} S
$\partial E_g / \partial \varepsilon$	-40 meV/%strain

under strain can be expressed as

$$G_{\text{MoS}_2}(\varepsilon) = G_0 \exp \left[-\frac{\varepsilon}{2k_B T} \frac{\partial E_g}{\partial \varepsilon} \right] \quad (2)$$

where G_0 stands for the conductance of the unstrained MoS₂ flake, k_B is the Boltzmann constant and T is the temperature. The measured conductance of the device is represented by black dots in Fig. 5(b). The fit of Eq. 1 and Eq. 2, obtained with experimental data is represented by red solid line in Fig. 5(b) showing a good agreement between experiment and model. The fitting parameters are reported in Table I, which are in very good agreement with literature[20].

We have also calculated the gauge factor for the present MSM device at $V_p=0.2$ V ($[\Delta I(\varepsilon)/I(0)]/\Delta\varepsilon$) to be ~ 110 in the range 5-10% of strain. The obtained value exceeds the values of conventional and other 2D based strain sensor, like graphene based devices[21].

In conclusion, we have measured the semiconductor-metal transition under monoaxial tensile strain of a 7 layer MoS₂ ribbon. An increase of more than an order of magnitude of the current flowing through the device, and a linear I-V relation are obtained at $\varepsilon=0.014$. A sound model of the conductance as function of the applied strain is given showing a good agreement between experimental data and theory.

AUTHOR INFORMATION

Author Contributions

I.N. and M.L.S. contributed equally to this work.

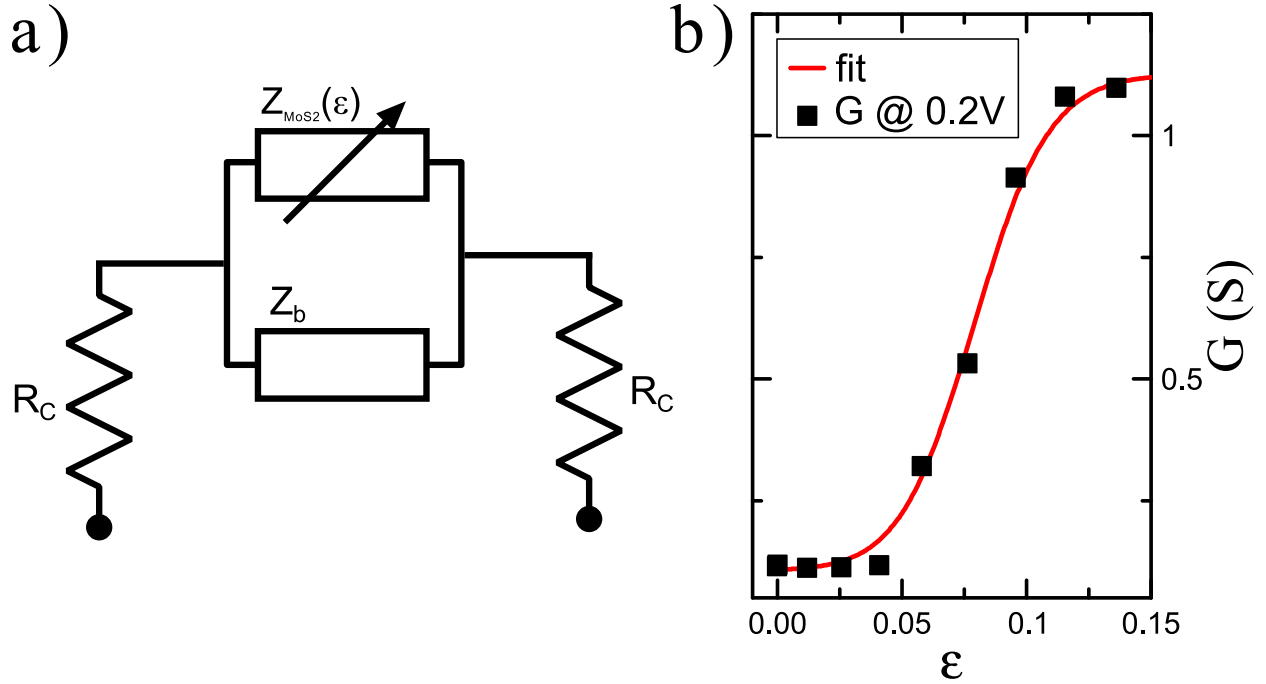


FIG. 5. Conductance of the device. a) Schematic of the device equivalent circuit formed by two resistive contacts in series with two parallel impedance representing the semiconductor part of the device. b) Measured (black squares) and modeled (solid red line) conductance of the device at $V_p=0.2$ V.

ACKNOWLEDGMENTS

The authors gratefully acknowledge W. Venstra for useful discussion, A. Di Michele and P. Sassi for Raman analysis. The authors acknowledge financial support from the European Commission (FPVII, Grant agreement no: 318287, LANDAUER).

* igor.neri@nipslab.org, miquel.lopez@nipslab.org

- [1] S. Bertolazzi, J. Brivio, and A. Kis, ACS nano **5**, 9703 (2011).
- [2] Q. H. Wang, K. Kalantar-Zadeh, A. Kis, J. N. Coleman, and M. S. Strano, Nature nanotechnology **7**, 699 (2012).
- [3] W. Wu, L. Wang, Y. Li, F. Zhang, L. Lin, S. Niu, D. Chenet, X. Zhang, Y. Hao, T. F. Heinz, J. Hone, and W. Zhong Lin, Nature **514**, 470 (2014).

- [4] E. Scalise, M. Houssa, G. Pourtois, V. Afanasev, and A. Stesmans, Nano Research **5**, 43 (2012).
- [5] P. Johari and V. B. Shenoy, ACS nano **6**, 5449 (2012).
- [6] M. Ghorbani-Asl, S. Borini, A. Kuc, and T. Heine, Physical Review B **87**, 235434 (2013).
- [7] H. J. Conley, B. Wang, J. I. Ziegler, R. F. Haglund Jr, S. T. Pantelides, and K. I. Bolotin, Nano letters **13**, 3626 (2013).
- [8] W. S. Yun, S. Han, S. C. Hong, I. G. Kim, and J. Lee, Physical Review B **85**, 033305 (2012).
- [9] M. López-Suárez, I. Neri, and R. Rurali, Journal of Applied Physics **119**, 165105 (2016).
- [10] H. Li, J. Wu, Z. Yin, and H. Zhang, Accounts of chemical research **47**, 1067 (2014).
- [11] H. Li, Z. Yin, Q. He, H. Li, X. Huang, G. Lu, D. W. H. Fam, A. I. Y. Tok, Q. Zhang, and H. Zhang, small **8**, 63 (2012).
- [12] A. Castellanos-Gomez, M. Buscema, R. Molenaar, V. Singh, L. Janssen, H. S. van der Zant, and G. A. Steele, 2D Materials **1**, 011002 (2014).
- [13] A. Castellanos-Gomez, R. Roldán, E. Cappelluti, M. Buscema, F. Guinea, H. S. J. van der Zant, and G. A. Steele, Nano Letters **13**, 5361 (2013).
- [14] H. Li, Q. Zhang, C. C. R. Yap, B. K. Tay, T. H. T. Edwin, A. Olivier, and D. Baillargeat, Advanced Functional Materials **22**, 1385 (2012).
- [15] A. Splendiani, L. Sun, Y. Zhang, T. Li, J. Kim, C.-Y. Chim, G. Galli, and F. Wang, Nano letters **10**, 1271 (2010).
- [16] J. M. Soler, E. Artacho, J. D. Gale, A. García, J. Junquera, P. Ordejón, and D. Sánchez-Portal, Journal of Physics: Condensed Matter **14**, 2745 (2002).
- [17] J. P. Perdew, K. Burke, and M. Ernzerhof, Physical review letters **77**, 3865 (1996).
- [18] K. F. Mak, C. Lee, J. Hone, J. Shan, and T. F. Heinz, Physical Review Letters **105**, 136805 (2010).
- [19] C. Ataca, M. Topsakal, E. Akturk, and S. Ciraci, The Journal of Physical Chemistry C **115**, 16354 (2011).
- [20] S. Manzeli, A. Allain, A. Ghadimi, and A. Kis, Nano letters **15**, 5330 (2015).
- [21] M. Huang, T. A. Pascal, H. Kim, W. A. Goddard III, and J. R. Greer, Nano letters **11**, 1241 (2011).